J|A|C|S ARTICLES

Published on Web 08/10/2009

Origin of Photocatalytic Activity of Nitrogen-Doped TiO_2 Nanobelts

Jin Wang,[†] De Nyago Tafen,[‡] James P. Lewis,[‡] Zhanglian Hong,[§] Ayyakkannu Manivannan,[‡,#] Mingjia Zhi,[†] Ming Li,[†] and Nianqiang Wu*[,†]

Department of Mechanical and Aerospace Engineering, WVNano Initiative, West Virginia University, Morgantown, West Virginia 26506-6106, Department of Physics, West Virginia University, Morgantown, West Virginia 26506, State Key Laboratory of Silicon Materials, Department of Materials Science & Engineering, Zhejiang University, Hangzhou 310027, P.R. China, and National Energy Technology Laboratory, U.S. Department of Energy, Morgantown, West Virginia 26507

Received May 9, 2009; E-mail: nick.wu@mail.wvu.edu

Abstract: Experiments combined with the density functional theory (DFT) calculation have been performed to understand the underlying photocatalysis mechanism of the nitrogen-doped titania nanobelts. Nitrogen-doped anatase titania nanobelts are prepared via hydrothermal processing and subsequent heat treatment in NH_3. Both the nitrogen content and the oxygen vacancy concentration increase with increasing the NH_3 treatment temperature. Nitrogen doping leads to an add-on shoulder on the edge of the valence band, the localized N 2*p* levels above the valence band maximum, and the 3*d* states of Ti^{3+} below the conduction band, which is confirmed by DFT calculation and X-ray photoelectron spectroscopy (XPS) measurement. Extension of the light absorption from the ultraviolet (UV) region to the visible-light region arises from the N 2*p* levels near the valence band and from the color centers induced by the oxygen vacancies and the Ti^{3+} species. Nitrogen doping allows visible-light-responsive photocatalytic activity but lowers UV-light-responsive photocatalytic activity. The visible-light photocatalytic activity originates from the N 2*p* levels near the valence band. The oxygen vacancies and the associated Ti^{3+} species act as the recombination centers for the photoinduced electrons and holes. They reduce the photocatalytic activity although they contribute to the visible light absorbance.

1. Introduction

Extensive efforts have been made to study titanium dioxide based photocatalysts due to their wide applications in environmental remediation and solar energy conversion.[1−3] However, the relatively large band gap of TiO_2 (3.2 eV for the anatase phase and 3.0 eV for the rutile phase) requires ultraviolet (UV) light for electron−hole separation, which is only 5% of the natural solar light. It is of great significance to develop photocatalysts that can be used in both UV irradiation (290−400 nm) and visible light (400−700 nm) to enhance the photocatalysis efficiency. One approach is to dope various transition-metal cations (such as V, Cr, Mn, Fe, and Ni) into TiO_2 at the Ti sites.[3−7] However, such cationic doping leads to the localized *d*-states deep in the band gap of TiO_2, which usually act as the recombination centers for photoexcited electrons and holes, leading to lower photocatalytic activity.[4,5] Also, cationic doping might unfavorably shift the conduction band below the redox potential of adsorbates, rendering the material inactive for photocatalysis. Another approach is to dope TiO_2 with anions such as N, C, S, and B,[8−11] which results in the *p*-states near the valence band much like other deep donor levels in semiconductors. Nitrogen doping has been shown to extend the light absorption onset from 380 nm to visible light (usually above 500 nm) and to offer possible photocatalytic activity under visible light irradiation.[9,12,13] However, some questions regarding the N-doped TiO_2 photocatalyst still remain unclear. These include the following:

(1) What is the underlying mechanism of the visible light response? Asahi et al.[9] have proposed that the band gap becomes narrow due to the hybridization of the N 2*p* state of the dopant with the O 2*p* valence band of TiO_2. Hence N doping will not cause the recombination of

[†] Department of Mechanical and Aerospace Engineering, West Virginia University.
[‡] Department of Physics, West Virginia University.
[§] Zhejiang University.
[#] National Energy Technology Laboratory, U.S. Department of Energy.

(1) Linsebigler, A. L.; Lu, G.; Yates, J. T., Jr. *Chem. Rev.* **1995**, *95*, 735.
(2) Hoffmann, M. R.; Martin, S. T.; Choi, W.; Bahnemann, D. W. *Chem. Rev.* **1995**, *95*, 69.
(3) Borgarello, E.; Kiwi, J.; Graetzel, M.; Pelizzetti, E.; Visca, M. *J. Am. Chem. Soc.* **1982**, *104*, 2996.
(4) Choi, W.; Termin, A.; Hoffmann, M. R. *J. Phys. Chem.* **1994**, *98*, 13669.
(5) Henderson, M. A.; White, J. M.; Uetsuka, H.; Onishi, H. *J. Am. Chem. Soc.* **2003**, *125*, 14974.
(6) Anpo, M.; Takeuchi, M. *Int. J. Photoenergy* **2001**, *3*, 1.
(7) Anpo, M.; Takeuchi, M. *J. Catal.* **2003**, *216*, 505.
(8) Sato, S. *Chem. Phys. Lett.* **1986**, *123*, 126.
(9) Asahi, R.; Morikawa, T.; Ohwaki, T.; Aoki, K.; Taga, Y. *Science* **2001**, *293*, 269.
(10) Sakthivel, S.; Kisch, H. *Angew. Chem., Int. Ed.* **2003**, *42*, 4908.
(11) Fujishima, A.; Zhang, X.; Tryk, D. A. *Surf. Sci. Rep.* **2008**, *63*, 515.
(12) Morikawa, T.; Asahi, R.; Aoki, K.; Taga, Y. *Jpn. J. Appl. Phys. Part 2* **2001**, *40*, L561.
(13) Lindgren, T.; Mwabora, J. M.; Avendano, E.; Jonsson, J.; Granqvist, C. G.; Lindquist, S. E. *J. Phys. Chem. A* **2003**, *107*, 5709.

 10.1021/ja903781h CCC: $40.75

photoexcited charge carriers. In contrast, other calculations have shown that no band gap narrowing occurs in the N-doped TiO_2. Instead N-doping induces localized N 2*p* states within the band gap just above the valence band maximum of TiO_2.[14−16]

(2) Does nitrogen doping induce other defect states like Ti 3*d* in the band gap that is usually associated with oxygen vacancies?

(3) How does nitrogen doping affect the UV-excited photocatalytic activity although it extends the light absorption to the visible region? In a desirable case, nitrogen doping should enhance the UV-responsive photocatalytic activity instead of diminishing it. Few studies have been performed on the UV-responsive photocatalytic activity of N-doped TiO_2.[17]

(4) Is the photocatalytic activity of the highly N-doped TiO_2 different from that of the slightly N-doped TiO_2? Based on the calculation by Asahi et al.,[9] band gap narrowing will occur when a high concentration of oxygen sites (6−12.5 at%) are substituted by nitrogen. In contrast, Okato et al.[18] have claimed that band gap narrowing does not occur in the TiO_2 doped with a high concentration of nitrogen atoms.

To clarify the above-mentioned questions, pristine anatase TiO_2 nanobelts are synthesized by hydrothermal processing and subsequently heat treated in NH_3 to allow nitrogen atom doping into the TiO_2 lattice in the present work. The nitrogen concentration in the TiO_2 nanobelts is controlled by modulating the heat-treatment temperature. The photocatalytic activities of the N-doped TiO_2 nanobelts under the ultraviolet A (UVA) and the visible-light irradiations are evaluated by monitoring the degradation of methyl orange in an aqueous solution. The chemical status of the nitrogen dopant and the electronic structure of the N-doped TiO_2 nanobelts have been studied using the optical/photoemission spectroscopy combined with the density functional theory (DFT) simulation. The origin of the visible-light response and the dependence of the photocatalytic activity on the N-dopant concentration are discussed.

In the present work, single-crystalline TiO_2 nanobelts are chosen as the test material, because one-dimensional (1D) nanostructures such as nanobelts, nanowires, and nanotubes have advantages over commonly used nanospheres or nanoparticles: (i) visible light scattering and absorption are highly enhanced in nanowires due to their high length-to-diameter ratio;[19] (ii) the 1D geometry facilitates rapid, diffusion-free electron transport along the longest direction;[20] and (iii) the high degree of crystallinity of the nanowires/nanobelts and the low number of grain boundaries may exhibit lower recombination rates. It is well-known that grain boundaries often act as the hole−electron recombination sites.

2. Experimental Section

2.1. Synthesis of the N-Doped TiO_2 Nanobelts. The synthesis of pristine anatase TiO_2 nanobelts are described in detail in our previous paper.[21] Briefly, 1.2 g of anatase titanium dioxide particles (Alfa Aesar) were added to 80 mL of 10 M NaOH aqueous solution. The mixture was vigorously stirred for 1 h and then transferred to a 100 mL Teflon-lined stainless steel autoclave. The autoclave was sealed and put into a preheated oven to perform hydrothermal treatment at 200 °C for 24 h. After hydrothermal processing, a white fluffy powder was collected and washed with copious amounts of deionized water and 0.1 M hydrochloric acid until the pH of the washing solution was less than 7. This resulted in the $H_2Ti_3O_7$ nanobelts.[21] This product was then dried in an oven at 80 °C overnight. The samples were then heated in a quartz tube furnace at 700 °C for 30 min at a ramp rate of 1 °C/min. As a result, the pristine single-crystalline anatase TiO_2 nanobelts were obtained.[21] Subsequently, anatase TiO_2 nanobelts were heat treated in an NH_3 flow in a tubular furnace equipped with a gas flow controller. Four N-doped samples were obtained by NH_3 treatment at different temperatures ranging from 525 to 600 °C for 3 h at a ramp rate of 10 °C/min. The pristine sample was also annealed at 550 °C in ambient air for comparison.

2.2. Characterization of the Nanobelts. The crystal structure of samples was characterized by powder X-ray diffraction (XRD) (X'Pert Pro PW3040-Pro, Panalytical Inc.) using Cu Kα radiation. The morphology was observed with a Hitachi S4700 field-emission scanning electron microscope (FE-SEM). For typical SEM sampling, 1 mg of nanobelts was added into 5 mL of absolute ethanol and then sonicated for 10 min to achieve a homogeneous whitish suspension. The suspension can stay stable for several days without obvious settling at the bottom of the container. The suspension was then dropped onto a smooth silicon wafer substrate (SPI Inc.) using a pipet and dried naturally in air. The dry powder specimen on the Si wafer was observed under SEM.

The UV−vis absorption spectra were measured under the diffuse reflection mode using the integrating sphere (UV2401/2, Shimadzu) attached to a Shimadzu 2550 UV−vis spectrometer. The powders were pressed to form a pellet and placed on a $BaSO_4$ plate. The use of the diffuse reflection mode for solid pellets effectively excluded the artifacts and inferences from the variation due to the inhomogenity and dispersion of nanoparticles in liquid.

The XPS experiments were performed on the titania nanobelts with PHI 5000 Versa Probe system (Physical Electronics, MN). The TiO_2 nanobelts were pressed to form a pellet prior to XPS measurement. The binding energy of the XPS spectra was calibrated with the reference to the C 1*s* peak at 284.8 eV.

2.3. Testing of the Photocatalysts. A commercial photoreactor (LUZ-4 V, Luzchem) equipped with fourteen 8 W lamps was used. The lamps centered at 350 nm (LZC-UVA, Luzchem) were employed for UVA irradiation, and the Vis-420 lamp centered at 420 nm (LZC-420, Luzchem) was for visible-light irradiation. The photocatalytic activity was evaluated by the decomposition of methyl orange in a deionized water solution with an initial concentration of 20 mg/L. A total of 0.01 g of catalysts was added to 10 mL of methyl orange solution in a 10 mL polyethylene tube. Before irradiation, the suspensions were sonicated in the dark for 5 min. During the radiation, the tubes were placed onto a carousel to ensure even exposure of every tube to the light. After desired time intervals of irradiation, the tubes were unloaded and centrifuged at 10 000 rpm for 1.5 h to separate the supernatant liquid from the catalysts. The supernatant liquid was collected and analyzed by recording the characteristic absorption of methyl orange (464 nm)

(14) DiValentin, C.; Pacchioni, G.; Selloni, A. *Phys. Rev. B* **2004**, *70*, 085116.
(15) Lee, J. Y.; Park, J.; Cho, J. H. *Appl. Phys. Lett.* **2005**, *87*, 011904.
(16) Batzil, M.; Morales, E. H.; Diebold, U. *Phys. Rev. Lett.* **2006**, *96*, 026103.
(17) Irie, H.; Watanabe, Y.; Hashimoto, K. *J. Phys. Chem. B* **2003**, *107*, 5483.
(18) Okato, T.; Sakano, T.; Obara, M. *Phys. Rev. B* **2005**, *72*, 115124.
(19) (a) Tan, B.; Wu, Y. *J. Phys. Chem. B* **2006**, *110*, 15932. (b) Zhu, K.; Neale, N. R.; Miedaner, A.; Frank, A. J. *Nano Lett.* **2007**, *7*, 69.
(20) (a) Adachi, M.; Murata, Y.; Takao, J.; Jiu, J.; Sakamoto, N.; Wang, F. *J. Am. Chem. Soc.* **2004**, *126*, 14943. (b) Baxter, J. B.; Aydil, E. S. *Appl. Phys. Lett.* **2005**, *86*, 053114. (c) Varghese, O. K.; Gong, D.; Paulose, M.; Ong, K. G.; Dickey, E. C.; Grimes, C. A. *Adv. Mater.* **2003**, *15*, 624. (d) Wu, N. Q.; Zhao, M.; Zheng, J.-G.; Jiang, C.; Myers, B.; Chyu, M.; Li, S.; Mao, S. X. *Nanotechnology* **2005**, *16*, 2878.
(21) Wang, J.; Wu, N. Q. In *Nanotechnology Research Advances*; Huang, X., Ed.; Nova Science Publishers: New York, 2008.

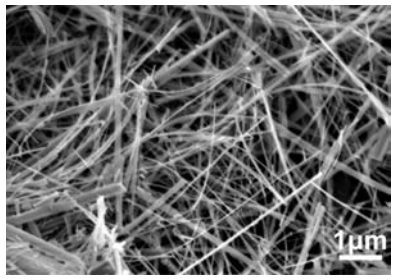

Figure 1. SEM image of the pristine TiO_2 nanobelts.

using the UV−vis spectrometer. The value of decomposition efficiency was calculated, based on the standard absorption curve of concentration and absorption. For the photocatalysis experiments including methanol into the system, 0.2 mL of methanol were added into 9.8 mL of TiO_2 aqueous suspension containing methyl orange to perform the same procedure. The experiments including oxygen and nitrogen into the system using the as-prepared 10 mL aqueous suspension containing methyl orange and TiO_2 was bubbled with the gas for 20 min using a syringe needle tip connected to a gas flow controller.

2.4. Computational Methods and Models. FIREBALL, an *ab initio* tight binding code based on density functional theory (DFT) with nonlocal pseudopotentials within the local density approximation (LDA)[22] was used to simulate the density of state (DOS) in TiO_2. In this method, the confined atomic-like orbitals were employed as a basis set for the determination of the occupied eigenvalues and eigenvectors of the one-electron Hamiltonian. For the calculations, a minimal basis set was chosen for N, O, and Ti, adding an excited *p*-state for polarization to the Ti ground-state configuration. This method has been successfully used for obtaining geometries and electronic properties of bulk TiO_2 material[23] as well as TiO_2 nanobelts.[24]

The atomic structure of the nanobelt was carved out from the anatase structure, which was found to be active in light absorption and photon-to-current conversion and was the prevalent one in experiments.[25] For each nanobelt the stoichiometry was preserved and no saturation of dangling bonds or charge embedding was applied. However, due to a long optimization procedure, surface atoms reconstruct and consequently are electronically passivated giving rise to a band gap free of surface states. The initial geometries were then fully optimized to the nearest local minimum structure. Based on the optimized geometries, nitrogen-doped TiO_2 nanobelts were constructed by embedding a few nitrogen atoms in the interspaces of the supercell. Oxygen vacancies were formed by removing a few oxygen atoms from the supercell. The resulting structures, $TiO_{2-x}N_y$ ($0.0 \leq x,y \leq 0.013$), were then fully relaxed and analyzed through electronic properties, a fundamental ingredient in photocatalysis.

Figure S1 shows a segment of a TiO_2 nanobelt comprising 96 TiO_2 units in the anatase phase. The dominant-area facet of the nanobelt is (101) which is stable and very reactive. The unit cells were repeated along the [010] direction to assemble the nanobelts.

3. Results and Discussions

3.1. Characterization of Morphology and Crystal Structure of the Nanobelts. Figure 1 shows the SEM image of the pristine TiO_2 nanobelts after hydrothermal processing and calcination.

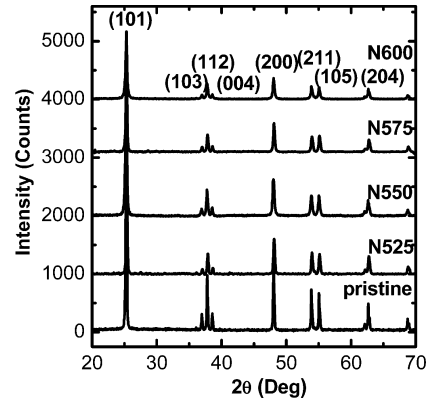

Figure 2. XRD patterns of the TiO_2 nanobelts before and after heat treatment in ammonia flow at different temperatures.

Table 1. XPS Peak Position and the N Content after Treatment of TiO_2 Nanobelts in NH_3 at Different Temperatures

sample	treatment temperature (°C)	N content (at%)	N 1s peak position (eV)	Ti $2p_{3/2}$ peak position (eV)	O 1s peak position (eV)
pristine	--	--	--	458.7	530.3
N525	525	0.30	399.6	458.5	529.8
N550	550	1.05	399.5	458.2	529.5
N575	575	1.20	399.7	458.1	529.5
N600	600	1.53	399.6/ 395.6	458.1	529.5

The nanobelts were 50−400 nm wide and up to tens of micrometers long. XRD analysis revealed that the pristine TiO_2 nanobelts have a monolithic anatase structure (Figure 2). The nanobelts were anatase single crystals with the growth direction along [010] and the two dominant surface facets as the (101) crystalline plane, as confirmed by transmission electron microscope (TEM) analysis (Figure S2 in Supporting Information). The nanobelts treated in NH_3 flow are denoted as N525, N550, N575, and N600, respectively. For example, N525 was the sample after NH_3 treatment at 525 °C. The pristine anatase TiO_2 nanobelts were pure white. N525, N550, and N575 were yellow, and the color became dark yellow with an increase in the heat treatment temperature. N600 showed a grayish green color. All the NH_3-treated samples retained a monolithic anatase phase. No other nitrogen-containing compounds or other titania polymorphs were detected by XRD. Moreover, there was no evident change in the XRD peak position of anatase after treatment in NH_3. A major difference between the pristine and the doped samples was that the peak intensity decreased and the peaks were broadened after nitrogen doping, which could be clearly seen by comparing the patterns of N600 and the pristine nanobelts. The size and shape of the nanobelts did not show any evident change after treatment in NH_3. Thus it is inferred that the orderliness of the crystal lattice of the anatase decreased upon nitrogen doping.

3.2. Measurement of Chemical Status and Electronic Structure by XPS. XPS measurement was performed on the N-doped TiO_2 nanobelts. The XPS spectrum of the Ti 2P core level obtained from the pristine TiO_2 nanobelts exhibited a Ti $2P_{3/2}$ peak at 458.7 eV and an O 1s peak at 530.3 eV (Figures S3 and S4 in the Supporting Information). After treatment in NH_3 at 600 °C, the Ti $2P_{3/2}$ and the O 1s peaks shifted to 458.1 and 529.5 eV, respectively (as listed in Table 1). The shifts of Ti $2P_{3/2}$ and the O 1s peaks are mainly due to the introduction of oxygen vacancies into the TiO_2 lattice. At a temperature higher

(22) Lewis, J. P.; Glaesemann, K. R.; Voth, G. A.; Fritsch, J.; Demkov, A. A.; Ortega, J.; Sankey, O. F. *Phys. Rev. B* **2001**, *64*, 195103.
(23) (a) Wang, H.; Lewis, J. P. *J. Phys.: Condens. Matter* **2005**, *17*, L209. (b) Wang, H.; Lewis, J. P. *J. Phys.: Condens. Matter* **2006**, *18*, 421.
(24) Tafen, D. N.; Wang, J.; Wu, N. Q.; Lewis, J. P. *Appl. Phys. Lett.* **2009**, *94*, 093101.
(25) Mor, G. K.; Varghese, O. K.; Paulose, M.; Shankar, K.; Grimes, C. A. *Sol. Energy Mater. Sol. Cells* **2006**, *90*, 2011.

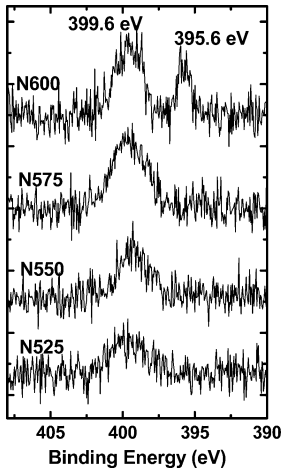

Figure 3. XPS spectra of the N 1*s* core level obtained from the anatase TiO_2 nanobelts after heat treatment in ammonia flow at different temperatures.

than 550 °C, NH_3 is decomposed, releasing H_2. This reducing atmosphere can cause partial reduction of TiO_2. It has been reported that the reduction of stoichiometric TiO_2 resulted in the shifts of both the Ti $2P_{3/2}$ and the O 1s peaks to lower binding energies.[26] In addition, the density functional theory (DFT) calculation has drawn a conclusion that nitrogen doping induces a substantial reduction of the formation energy of oxygen vacancies in bulk TiO_2.[27] This indicates that nitrogen doping is accompanied by oxygen vacancy formation. On the other hand, it has been reported that the incorporation of N atom into the TiO_2 lattice can also lead to the shift of Ti $2P_{3/2}$ to lower binding energy.[28,29] Our XPS analysis determined that the nitrogen contents were 0.30 at% for Sample N525, 1.05 at% for N550, 1.20 at% for N575, and 1.53 at% for N600 (as shown in Table 1). As the heat-treatment temperature increased, the nitrogen doping level increased. There is a leap in the concentration from 0.3% for N525 to 1.05% for N550. This is due to the fact that the decomposition of NH_3 into N_2 and H_2 started at 550 °C.[17] The reducing atmosphere greatly facilitates the doping of nitrogen due to the formation of oxygen vacancies.

Figure 3 shows the N 1*s* XPS spectra of the pristine and the N-doped titania nanobelts. Two N 1*s* peaks are present in the spectra of N-doped samples. For all the N-doped samples, there is a peak at ~399.6 eV. For Sample N600, an additional peak appeared at 395.6 eV. The N 1*s* peak at 395.6 eV is characteristic of N^{3-} that corresponds to TiN.[30,31] The N 1*s* peak at 395−397 eV obtained from N-doped TiO_2 has also been assigned to the Ti−N bonding by other researchers.[18,32−34] The N 1*s* peak at ~399.6 eV is ascribed to Ti−O−N or Ti−N−O oxynitride. One may argue that this peak could also be assigned to N−H or adsorbed NH_3, because its binding energy is close to the value (398.7−399.7 eV) cited for NH_3.[30,35] In the present work, the N-doped samples were analyzed using Fourier Transform Infrared (FTIR) spectroscopy. No bands characteristic of N−H or NH_3 were found in the FTIR spectra (Figure S5 in the Supporting Information), which excludes the possibility that the peak at 399.6 eV is derived from N−H or adsorbed NH_3. This peak cannot be assigned to the NO_x molecules, because the N 1*s* binding energy for NO_x is typically larger than 403 eV.[30] Moreover, our FITR measurement did not detect any NO_x molecules.

Nitrogen can be located in the anatase lattice of TiO_2 interstitially or/and substitutionally. As summarized by Fujishima et al.,[11] the N 1*s* peak at ~400 eV is typically assigned to the interstitial nitrogen dopant while the peak at ~396 eV is ascribed to the substitutional nitrogen dopant. The site of the N atoms in the TiO_2 lattice depends on the synthetic route of N-doped TiO_2. Different synthetic routes make nitrogen species react with TiO_2 in different fashions. Di Valentin et al.[14] have performed DFT calculations of nitrogen doping behaviors on the single-crystalline anatase TiO_2 (101) surface. Their calculations have showed that transition from the substitutional to the interstitial nitrogen doping undergoes an exothermic process by 0.8 eV, which implies that substitutional nitrogen formation starting from the interstitial one will require more energy. Interstitial nitrogen doping is preferred under the oxygen-rich condition, whereas under oxygen-depleted conditions (at high reducing condition) after annealing at high temperature, substitutional N in parallel with oxygen vacancy is favored. In addition, it has been reported that, at high temperature, oxygen vacancies in a single-crystalline TiO_2 (110) surface occur at ~580 °C in a vacuum. Furthermore, the presence of nitrogen dopant facilitates the formation of oxygen vacancies.[16,36,37] In the present work, the pristine single-crystalline anatase TiO_2 nanobelts with the (101) crystal plane as the dominant surface facets were obtained by calcinations in air of hydrogen titanate ($H_2Ti_3O_7$). During calcinations, water molecules are released,[21] leading to numerous dangling oxygen bonds exposed on the surface, which creates an oxygen-rich surface. Therefore, at relatively low temperature, the nitrogen atoms tend to sit in the interstitial sites (all the nitrogen atoms were located in the interstitial sites when the N content was below 1.2 at%). At relatively high temperature (600 °C) under reducing atmospheric conditions (more H_2 are produced via decomposition of NH_3 at higher temperature), some of the nitrogen atoms are incorporated into the TiO_2 lattice substitutionally in addition to the presence of the interstitial nitrogen atoms. It is worth noting that the interstitial N atoms are limited in a very low range. Even at only 1.53 at% N, excessive N atoms were present in the substitutional sites after the N atoms at the interstitial site become saturated.

In summary, the present work reveals that interstitial nitrogen doping appears at a low nitrogen-dopant concentration at relatively low temperatures (525, 550, and 575 °C), while substitutional nitrogen atoms are also present in addition to the interstitial nitrogen dopant at relatively high temperature (in the

(26) Rumaiz, A. K.; Ali, B.; Ceylan, A.; Boggs, M.; Beebe, T.; Shah, S. I. *Solid State Commun.* **2007**, *144*, 334.
(27) Valentin, C. D.; Pacchioni, G.; Selloni, A.; Livraghi, S.; Giamello, E. *J. Phys. Chem. B* **2005**, *109*, 11414.
(28) Saha, N. C.; Tompkins, H. G. *J. Appl. Phys.* **1992**, *72*, 3072.
(29) Kitano, M.; Funatsu, K.; Matsuoka, M.; Ueshima, M.; Anpo, M. *J. Phys. Chem. B* **2006**, *110*, 25266.
(30) Moulder, J. F.; Stickle, W. F.; Sobol, P. E.; Bomben, K. D. *Handbook of X-ray photoelectron Spectroscopy*; Eden Prairie: 1992.
(31) Esaka, F.; Furuya, K.; Shimada, H.; Imamura, M.; Matsubayashi, N.; Sato, H.; Kawana, A.; Ichimura, H.; Kikuchi, T. *J. Vac. Sci. Technol., A* **1997**, *15*, 2521.
(32) Takahashi, I.; Payne, D. J.; Palgrave, R. G.; Egdell, R. G. *Chem. Phys. Lett.* **2008**, *454*, 314.
(33) Chen, H.; Nambu, A.; Wen, W.; Graciani, J.; Zhong, Z.; Hanson, J. C.; Fujita, E.; Rodriguez, J. A. *J. Phys. Chem. B* **2007**, *111*, 1366.
(34) Nambu, A.; Graciani, A. N.; Rodriguez, J. A.; Wu, Q.; Fujita, E.; Fdez-Sanz, J. *J. Chem. Phys.* **2006**, *125*, 094706.
(35) Jansen, R. J. J.; Van Bekkum, H. *Carbon* **1995**, *33*, 1021.
(36) Nakano, Y.; Morikawa, T.; Ohwaki, T.; Taga, Y. *Appl. Phys. Lett.* **2005**, *86*, 132104.
(37) Livraghi, S.; Paganini, M. C.; Giamello, E.; Selloni, A.; Valentin, C. D.; Pacchioni, G. *J. Am. Chem. Soc.* **2006**, *128*, 15666.

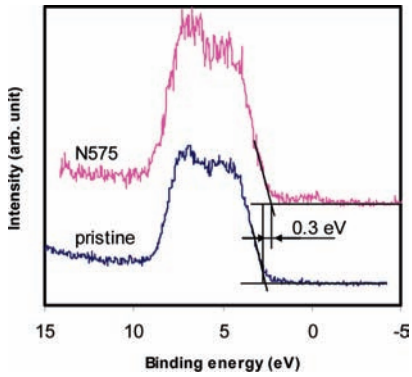

Figure 4. XPS spectra of TiO_2 nanobelts, showing the valence bands for the pristine and N575 sample (treated in NH_3 at 575 °C).

sample treated at 600 °C). The result obtained in the present work is in disagreement with that reported by Okato et al.[18] Okato et al. reported that, at a low concentration, the N atoms were doped into the O sites substitutionally. The N dopant became saturated in the substitutional sites as the concentration of N increases in TiO_2. As a result, the excessive N atoms were interstitially doped into the TiO_2 lattice. The controversy could be due to the difference in the synthesis route employed. They have employed a pulse-laser deposition method to make the N-doped TiO_2 film by using the mixed TiO_2 and TiN powders as the target.

Figure 4 shows the valence band spectra obtained from the pristine TiO_2 nanobelt sample and the N-doped sample (N575, treated at 575 °C). After nitrogen doping, the valence band edge has exhibited ~0.3 eV of red shift. Moreover, small bands occurred above the valence band maximum (VBM), and small bands existed close to the binding energy at zero.

3.3. Calculation of the Density of States (DOS). The electronic structures of the anatase TiO_2 nanobelts were further analyzed through calculated density of states. Figure 5a and 5b plot the density of states (DOS) and the projected DOS for the nitrogen-doped and the nitrogen−oxygen vacancy-containing nanobelts, respectively, and compared them with that of the pristine titanium oxide nanobelts. The calculated band gap of the pristine TiO_2 nanobelt was 3.42 eV compared to the experimental value 3.26 eV derived from the UV−visible spectrum (Figure 6). The use of a local orbital basis set in our calculations compensates for the underestimating effect of the LDA on the optical gap.[23] The difference between the calculated and experimental band gaps is a quantum confinement effect due to the size of the calculated nanobelts compared to the experiments. For the pristine titanium oxide nanobelts (Figure 5a), the valence band (VB) and the conduction band (CB) consist of both the O 2*p* and Ti 3*d* states as in the case of the bulk.[38] As nitrogen atoms are doped into TiO_2, the N 2*p* states are delocalized (see Figure S6 in the Supporting Information) and significantly contribute to the formation of impurity energy levels hybridized by O 2*p* states and Ti 3*d* states. For the interstitial nitrogen-doped nanobelts in the absence of oxygen vacancies (Figure 5a), two isolated impurity levels are located above the valence band maximum (VBM). The contribution of N 2*p* states to these impurity energy levels increase with an increase in the nitrogen concentration (Figure 5a). In addition, an add-on shoulder is present on the edge of the VBM.

(38) Asahi, R.; Taga, Y.; Mannstadt, W.; Freeman, A. J. *Phys. Rev. B* **2000**, *61*, 7459.

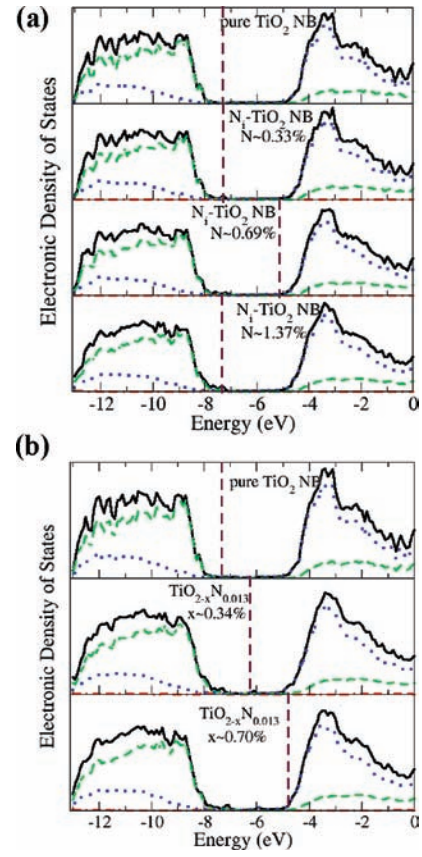

Figure 5. Calculated density of state (DOS) and the species-projected DOS (the dashed lines indicate the position of the Fermi level); (a) TiO_2 with various nitrogen concentrations of dopant (0.33, 0.69, and 1.37 at%) in the absence of the oxygen vacancy; (b) N-doped TiO_2 with a fixed nitrogen concentration (1.3 at%) in the presence of different concentrations of oxygen vacancies ($x = 0.0034, 0.0070$). Black solid line, total DOS; green dash line, O 2*p* states; blue dot line, Ti 3*d* states; red dash line, N 2*p* states.

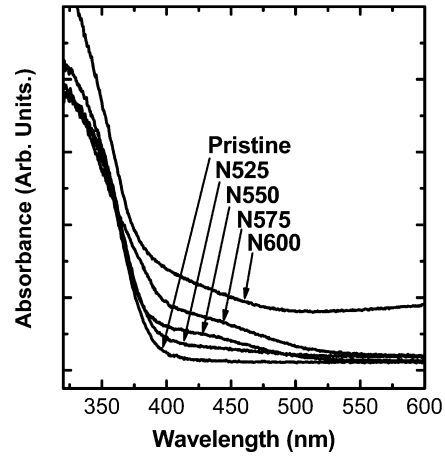

Figure 6. Diffuse reflectance spectra of the anatase TiO_2 nanobelts before and after heat treatment in ammonia gas flow at different temperatures.

When N-doping is accompanied by the presence of the oxygen vacancies, an additional deep donor level is introduced below the conduction band minimum (CBM) (Figure 5b). The number of impurity energy levels depends on the concentration of oxygen vacancies in the nitrogen-doped nanobelts (Figure 5b). These energy levels mainly consist of the 3*d* states of Ti^{3+}. The deep donor level was located at a distance of 1.28 and 1.20 eV from the CBM for the oxygen vacancy concentrations of

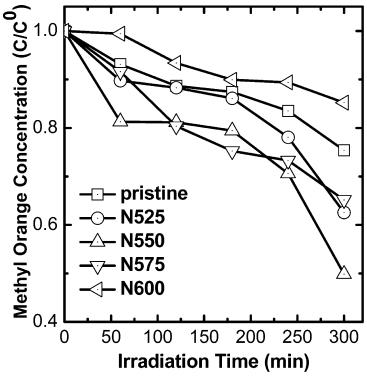

Figure 7. Photocatalytic activities of the titania nanobelts under visible light irradiation.

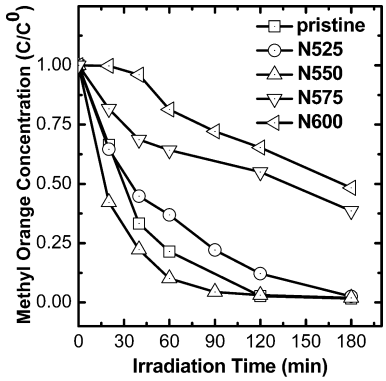

Figure 8. Photocatalytic activities of the titania nanobelts under UVA irradiation.

0.34% and 0.70%, respectively. In summary, when both the nitrogen atoms and the oxygen vacancies are present in the lattice of the anatase titanium oxide nanobelts, several local states appear in the band gap besides the presence of an add-on shoulder on the tail of the VBM, which are consistent with the small bands above the VBM detected in the XPS spectrum of the nitrogen-doped anatase titanium oxide nanobelts.

3.4. Measurement of the Light Absorption. Figure 6 shows the UV−visible spectra of the pristine and the nitrogen-doped titania nanobelts. For the pristine anatase TiO_2 nanobelts, the absorption spectrum was cut off at ∼380 nm, from which the band gap of the pristine titania nanobelt was estimated to be 3.26 eV. For the N-doped nanobelts, an add-on shoulder was imposed onto the cutoff edge of the absorption spectrum, which extended the absorption from 380 to 550 nm. The absorbance intensity in the wavelength range from 380 to 550 nm increased as the NH_3 treatment temperature increased. Such light absorbance enhancement in the near-UV region and in the visible-light range was consistent with the yellow color characteristic of the N-doped titania samples.

The extension of the light absorption from the UV to the visible range arises from the contributions of both the doped nitrogen atoms and the oxygen vacancies in the lattice, because the interstitial nitrogen atoms induced the local states near the valence band edge and the oxygen vacancies give rise to the local states below the conduction edge. Excitation from such local states to the conduction band is consistent with the "add-on shoulder" on the absorption edge of the UV−visible spectrum. Recently Serpone has proposed[39] that oxygen vacancies induced by cation doping in TiO_2 can act as the color center. The electrons left in the oxygen vacancies can also interact with adjacent Ti^{4+} to give the Ti^{3+} color center. The presence of these color centers in titania also contributes to the visible light absorption. Therefore, the samples are treated at higher temperatures, and more oxygen vacancies are created due to higher N dopant content, as discussed in the previous sections. Therefore, the visible light absorbance is higher for the samples treated at higher temperature.

3.5. Evaluation of the Photocatalytic Activities. The photocatalytic activities of the nanobelts were evaluated by monitoring the decomposition of methyl orange in an aqueous solution under visible light and UV irradiation, respectively. The direct decomposition of methyl orange without the presence of photocatalysts was not detected under visible light irradiation in a control experiment. Figure 7 shows the degradation curve of methyl orange catalyzed by the pristine and the N-doped titania nanobelts under visible light irradiation. A trend in the photocatalytic activity has been observed in the following order: N550 > N575 > N525 > pristine > N600. The feeble response of the pristine sample to visible light might be due to its intrinsic oxygen vacancy or other reasons. The photocatalytic activity of the N-doped nanobelts upon visible light irradiation increased with the N content except for Sample N600. Figure 8 shows the decomposition curves of methyl orange catalyzed by the nanobelts upon UV exposure. As compared to the photocatalytic activity of pristine sample, Sample N550 demonstrates a slightly enhanced activity while N525 shows a slightly reduced activity. In contrast, N575 and N600 exhibit a significant reduction of the photocatalytic activity. Sample N600, which has the highest nitrogen concentration, exhibited the lowest activity under both visible light and UV irradiation.

When the energy of an incident light exceeds the band gap of the photocatalyst during the photocatalysis process, electrons in the valence band will be excited into the conduction band, leaving holes in the valence band. The electrons and holes will be further transferred to the photocatalyst surface. Subsequently the charge carriers can form reactive oxygen species (ROS). Typically, the photogenerated electrons combine with adsorbed oxygen to form superoxide anions ($O_2^{\bullet -}$), and the holes react with OH^- to form hydroxyl radicals ($OH^{\bullet}$).[1] The photogenerated charge carriers or ROS will react with reactants. To examine the roles of the photogenerated electrons and holes in photocatalysis of methyl orange, comparative experiments were performed by incorporating methanol, oxygen gas, and nitrogen into the photoreactor. Here methanol acted as the scavenger for the photogenerated holes. Oxygen can trap the photogenerated electrons to generate superoxide anions. And nitrogen can deplete the oxygen content in the solution. Figure 9 shows the degradation curve of methyl orange catalyzed by Sample N575 under visible light irradiation in the absence and presence of methanol, oxygen, and nitrogen, respectively. When methanol is present around the TiO_2 surface, it will actively scavenge the holes photogenerated from the valence band and, thus, suppress the formation of surface hydroxyl radicals. In fact, no evident change in the photocatalysis rate of the system was observed after methanol was added into the solution. This indicated that the photogenerated holes or the hydroxyl radicals did not play a major role in decomposing methyl orange. In contrast, the photocatalysis rate of the system was significantly reduced by saturating the aqueous solution with nitrogen to deplete the oxygen in the solution. This suggests that oxygen plays an important role in degrading methyl orange. Saturating

(39) Serpone, N. *J. Phys. Chem. B.* **2006**, *110*, 24287.

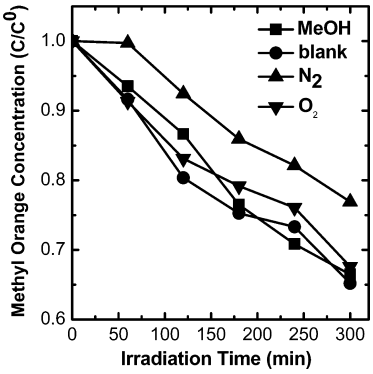

Figure 9. Photocatalytic activity of Sample N575 under visible-light irradiation in the absence (the curve denoted as "blank") and presence of methanol, oxygen, and nitrogen, respectively.

the aqueous solution with oxygen neither enhanced nor reduced the photocatalysis rate. Therefore, the generation of electrons and superoxide anions by incident light irradiation is the rate-limiting step during photocatalysis of the decomposition of methyl orange in the present investigation.

The overall photocatalytic activity depends on two factors: (i) the separation efficiency of electrons and holes and (ii) the recombination rate of the photogenerated electron−hole pairs. The holes or the surface hydroxyl radicals are generally viewed as major oxidizing agents for degrading reactants, while superoxide anions formed by scavenging the electrons from the conduction band are also capable of oxidizing reactants. In the present work, the superoxide anions are proposed to play a dominant role in photocatalysis as indicated in Figure 9. Based on the DOS calculation and XPS analysis results, the add-on shoulder on the edge of VBM is induced by the N 2*p* states and the local N 2*p* levels are present above the valence band maximum for the nitrogen-doped titania nanobelts. The electrons in these levels can be excited to the conduction band by visible light. These photogenerated electrons are bound to the adsorbed oxygen to produce superoxide anions, which leads to the photocatalytic activity under visible light irradiation. As inferred from the UV−vis spectra in Figure 6, the absorbance in the add-on shoulder increases as the nitrogen concentration goes up, and the electron generation rate also increases upon visible light irradiation as the nitrogen concentration rises, which leads to the enhanced photocatalytic efficiency. However, the holes in these N 2*p* deep levels induced by the interstitial N dopant are highly localized and, thus, have a very low mobility,[24] and consequently are barely involved in the photocatalysis.

The 3*d* states of Ti^{3+} below the conduction band at ~1.2 eV, in which Ti^{3+} are typically formed by trapping the electrons adjacent to the oxygen vacancy sites, can contribute to the visible light absorption as the color center. However, these levels act as electron−hole recombination centers, leading to the decrease in the photocatalytic activity. This is in agreement with the previous studies,[40,41] in which the Ti^{3+} sites associated with oxygen vacancies are considered as the recombination centers for the photoinduced electrons and holes. In the present work, the N content in the titania lattice increases with the heat treatment temperature, leading to an increase in the concentration of oxygen vacancies. Sample N600 with the highest N dopant content has the most oxygen vacancies and the most Ti^{3+} species. Furthermore, substitutional N atoms may cause additional Ti^{3+} species. Hence, it is not surprising that sample N600 exhibits the lowest photocatalytic activity.

For the N-doped nanobelts, only electrons in the N 2*p*-induced level right above the VBM can be excited to the conduction band under visible light irradiation. In contrast, the electrons both in the valence band and in the localized N 2*p* levels are excited to the conduction band under UV irradiation. The UV-induced charge carriers from the localized N 2*p* levels account for a very small percentage in comparison to those from the valence band. More charge carriers are generated in the N-doped titania nanobelts than the pristine titania sample under UV irradiation. However, the holes in the local N 2*p* states in the band gap, induced by N doping, are highly localized and, thus, have a very low mobility. These localized N 2*p* levels along with the 3*d* states of Ti^{3+} in the band gap act as the recombination centers for the charge carriers photoinduced from the valence band. In short, although N doping promotes the generation of charge carriers to some degree under UV irradiation (positive effect), it leads to a higher recombination rate (negative effect). Therefore, N-doping has a limited contribution to the enhancement of photocatalytic activity under UV irradiation. Sample N550 is the best among all the samples, which only demonstrates a slightly enhanced UV photoactivity. All other N-doped samples exhibit lower UV photocatalytic activity than the pristine titania nanobelts. In this case, the negative effect of the N doping dominates over the positive effect. An additional side effect of annealing in NH_3 at too a high temperature is the reduced crystallinity, which is confirmed by XRD analysis. The crystallinity of both Samples N575 and N600 is degraded as compared to the pristine sample. A lower crystallinity of titania is an additional reason for lower photocatalytic activity.[42]

4. Conclusions

The nitrogen-doped titania nanobelts were prepared by heat treatment in NH_3 at elevated temperatures. The N-doped nanobelts retained the anatase structure after exposure to NH_3 form at 525 to 600 °C. The nitrogen dopant level in the lattice increased with an increase in the NH_3 treatment temperature, accompanied with an increase in the oxygen vacancies. Nitrogen atoms were induced on the interstitial site at a low N doping level. At 1.53 at % level, the interstitial sites became saturated and extra N atoms were located on the substitutional sites in the anatase lattice.

XPS measurement and FIREBALL calculations of DOS have demonstrated that nitrogen doping induced an add-on shoulder on the edge of the valence band maximum and the localized N 2*p* states above the valence band. The 3*d* states of Ti^{3+} below the conduction band were also originated due to the presence of oxygen vacancies in the anatase lattice.

For the N-doped nanobelts, an add-on shoulder was imposed onto the cutoff edge of the UV−vis absorption spectra, which extended the absorption range from 380 to 550 nm. Visible light absorption is promoted from the N 2*p* levels near the valence band maximum, and the color centers are induced by the oxygen vacancies and the Ti^{3+} species. The higher N dopant level

(40) Takeda, S.; Suzuki, S.; Odaka, H.; Hosono, H. *Thin Solid Films* **2001**, *392*, 338.
(41) Ikeda, S.; Sugiyama, N.; Murakami, S.; Kominami, H.; Kera, Y.; Noguchi, H.; Uosaki, K.; Torimoto, T.; Ohtani, B. *Phys. Chem. Chem. Phys.* **2003**, *5*, 778.
(42) Wu, N. Q.; Wang, J.; Li, M.; Zhi, M.; Manivannan, A. *Mater. Res. Soc. Symp. Proc.* **2009**, *1144*, LL07–08.

resulted in a larger add-on shoulder on the absorption edge and an enhancement of absorbance in the overall visible region.

The visible light responsive photoactivity of the N-doped titania originated from the excited electrons from the N 2*p* states on the edge of the valence band maximum (VBM) and the local N 2*p* levels above the VBM. The 3*d* states of Ti^{3+} below the conduction band, which were associated with oxygen vacancies, acted as the electron−hole recombination centers, leading to the reduction of photocatalytic activity. For the N-doped titania nanobelts, only electrons in the N 2*p* levels above the VBM can be excited to the conduction band under visible light irradiation, while the electrons both in the valence band and in the localized N 2*p* levels were excited to the conduction band under UVA irradiation. When the N dopant content increased, more electrons were available to be excited from the localized N 2*p* levels near the valence band maximum while the oxygen vacancies and the associated Ti^{3+} species increased in the anatase lattice. Sample N600 exhibited the lowest photocatalytic activity due to the highest defect concentration.

Acknowledgment. This work is financially supported by an NSF grant (CBET-0834233), an ARTS grant from Eberly College of Arts and Sciences at West Virginia University, and the Research Challenge Grant of West Virginia State (EPS08-01). Some of the facilities and resources used in this work are supported by NSF Grant EPS 0554328 with matching funds from the West Virginia University Research Corporation and the West Virginia EPSCoR Office. We are grateful to Dr. Jianguo Zheng for his TEM measurements at Materials Characterization Center, LEXI/Calit2, University of California−Irvine.

Supporting Information Available: A segment of a relaxed nanobelt comprised of 96 TiO_2 units in the anatase phase is presented in Figure S1; HRTEM of the anatase titanium oxide nanobelts is shown in Figure S2; XPS spectra of the Ti 2P core level, the O 1s core level of the anatase nanobelts before and after nitrogen doping is shown in Figures S3 and S4, respectively; FTIR spectra of the anatase nanobelts before and after nitrogen doping is presented in Figure S5; Calculated density of state (DOS) for N 2p at different nitrogen contents in the anatase TiO_2 lattice is shown in Figure S6. This material is available free of charge via the Internet at http://pubs.acs.org.

JA903781H